AIAA JOURNAL
Vol. 35, No. 6, June 1997

Dusty Detonation Simulations with Adaptive Unstructured Finite Elements

E. Loth* and S. Sivier†
University of Illinois at Urbana–Champaign, Urbana, Illinois 61801
and
J. Baum‡
Science Applications International Corporation, McLean, Virginia 22102

A nonequilibrium reacting flow methodology has been combined with a conservative, monotonic, two-phase, compressible flow solver to allow numerical simulations of gas detonations subject to inert particles. This flow solver incorporates unstructured dynamically adaptive meshes with the finite element method–flux-corrected transport scheme for both the gas and particle phases. A simple two-step induction parameter model was used to model the combustion of the gas phase coupled with a point-implicit scheme for the energy release equation. This combustion model was then used to simulate two-dimensional detonation macroscopic features of a hypothetical fuel oxygen diluent mixture for a few sample cases. These simulations employed particles of various diameters and mass loadings resulting in both successful and failed detonations.

I. Introduction

TWO-PHASE reacting compressible flow phenomena present an important field of study for engineering systems, which include solid rocket motors, particle or droplet detonations, and sprays in hypersonic scramjet engines. When solving the compressible two-phase equations, the continuum gas dynamics are usually best represented by an Eulerian description, that is, the gas characteristics are calculated at fixed points within the flow. However, the particles can be modeled by either an Eulerian description (in the same manner as the gas flow) or a Lagrangian description (where individual particle groups are monitored and tracked in the flow). Whereas Lagrangian descriptions are better suited for turbulent dispersion and particle-reflection simulations, an Eulerian particle description allows improved interphase coupling accuracy by coincident description with the gas flow. Recently, we have investigated both Eulerian and Lagrangian methodologies of the particle phase for the problem of shock attenuation by inert particles by using unstructured finite element grids.[1,2] The results indicate that, for such flows, the Eulerian particle description provides a superior solution with respect to flow modulation because of the coincident nodal description of the gas flow characteristics and greater computational efficiency. Therefore, the Eulerian description is employed in the present study for both the particle and gas phases.

To date, there have been only a few fundamental experimental studies on gaseous detonations with inert particles. One such investigation by Laffitte and Bouchet[3] examined the prevention of detonations by particle addition. The study investigated decreasing the particle diameter while keeping the total mass of the particles per unit volume of air (mass loading) fixed. The results suggested that an increase in the total surface area of the particles enhanced the ability of the particles to prevent detonation. Additionally, it appeared that stoichiometric conditions required the greatest number of particles for detonation prevention. Kauffman et al.[4] experimentally examined dust (where the fuel is contained within the particles), hybrid (where the fuel is contained in both the particles and their surrounding gas), and dusty (where the particles are chemically inert) detonations. The dusty detonation results show that, for inert particles with large diameters or small mass loadings, the particles have little or no effect on detonation velocity. However, sufficiently small particles or sufficiently large loadings in the flow results in detonation failure.

In general, numerical studies of multidimensional dilute dusty two-phase detonations are scarce. Analytically, Kulikovskii[5] presented a quasi-one-dimensional study of gaseous detonations containing inert particles. The results indicate that it is the volume concentration of particles in the flow that plays a major role in modifying the flow rather than particle diameter (whereas the results of Kauffman et al.[4] show that changes in particle diameter were more critical). The present study seeks to establish a two-dimensional finite element methodology for efficiently simulating two-phase dusty detonations for finite reaction rates and the particle velocity and temperature in nonequilibrium with respect to the gas velocity and temperature. The proposed technique is a monotone-preserving algorithm coupled with unstructured adaptive grids for efficient resolution of reaction zones. A few sample simulations are conducted here to note the effect of particle conditions on detonation success.

II. Numerical Method

In modeling the flowfield, the following assumptions were incorporated: the particle volume fraction is negligible (ranging from 10^{-5} to 10^{-3} in this study) and the particles are spherical, inert, and of uniform size and temperature. The first assumption indicates that the particles are also dilute, i.e., particle–particle interactions do not account for a significant portion of the forces on the particles, and they do not significantly contribute to the gas pressure (because of the small volume fraction of the particles). Because the particle density ρ_p is more than three orders of magnitude larger than the surrounding gas density ρ, the added (or virtual) mass effect can be neglected. Because the gravity-induced terminal drag forces of the particles are far less than the shock-induced drag forces, gravitational effects are also neglected. Because lift-to-drag ratios are much less than one due to low vorticity (outside of contact discontinuities), the lift force is neglected. Because the gas velocity gradients through which the particles will be convected have scales much larger than the particle diameter (except at the shock), Basset history and Faxen terms are also neglected. Thus, the only forces acting on the particles (pressure and viscosity) can be described based on a single coefficient of drag. As for energy coupling, the effects of radiation can be considered negligible because phase temperature differences are not excessive; therefore, heat transfer can be expressed simply in convective terms based on a constant Prandtl number.

Received Aug. 29, 1996; revision received Feb. 7, 1997; accepted for publication Feb. 25, 1997.

*Associate Professor, Department of Aeronautical and Astronautical Engineering. E-mail: e-loth@uiuc.edu. Senior Member AIAA.

†Graduate Research Assistant, Department of Aeronautical and Astronautical Engineering; currently Mechanical Engineer Specialist, Lockheed Martin Missiles and Space Company, Inc., Orgn. V2-10, Building 157, 111 Lockheed Way, Sunnyvale, CA 94089. Member AIAA.

‡Senior Research Scientist. Member AIAA.

A. Gas and Particle Equations

The differential equations of the reacting gas and inert particles can be written similarly as

$$\frac{\partial \boldsymbol{U}}{\partial t} + \frac{\partial \boldsymbol{F}_j}{\partial x_j} = \boldsymbol{S} \qquad \frac{\partial \boldsymbol{U}_p}{\partial t} + \frac{\partial \boldsymbol{F}_{pj}}{\partial x_j} = \boldsymbol{S}_p \tag{1}$$

where the summation convention is used and where quantities with subscript p indicate a particle value. The gas equations for a two-phase flow as given by Ref. 1 are

$$\boldsymbol{U} = \begin{bmatrix} \rho \\ \rho u_i \\ \rho e \end{bmatrix} \qquad \boldsymbol{F}_j = \begin{bmatrix} \rho u_j \\ \rho u_i u_j + p\delta_j \\ u_j(\rho e + p) \end{bmatrix}$$

$$\boldsymbol{S} = \begin{bmatrix} 0 \\ -D_i \\ -Q - u_{pi} D_i \end{bmatrix} \tag{2}$$

where D_i is the component of drag force on the particles in the i direction of a Cartesian coordinate system per unit volume of gas, u_i is the component of the fluid velocity in the i direction, u_{pi} is the particle velocity in the i direction, and Q is the heat transferred from the gas to the particles per unit volume of gas. The constitutive equations used for drag and heat transfer are relatively standard and are discussed in detail in Ref. 1. The state equations were modified to include chemical energy as per Taki and Fujiwara[6]:

$$p = (\gamma - 1)\rho\left[e - \frac{1}{2}u_j u_j - \omega q\right] \qquad T = \frac{\left[e - \frac{1}{2}u_j u_j - \omega q\right]}{c_v}$$

where ρ, p, e, T, γ, c_v, ω, and q are density, pressure, specific total energy, temperature, ratio of specific heats, specific heat at constant volume, fraction of fuel remaining, and heat of reaction per unit mass, respectively.

The five particle equations[1] are

$$\boldsymbol{U}_p = \begin{bmatrix} \sigma \\ \sigma u_{pi} \\ \sigma e_p \\ n \end{bmatrix} \qquad \boldsymbol{F}_{pj} = \begin{bmatrix} \sigma u_{pj} \\ \sigma u_{pi} u_{pj} \\ u_{pj}\sigma e_p \\ n u_{pj} \end{bmatrix}$$

$$\boldsymbol{S}_p = \begin{bmatrix} 0 \\ D_i \\ Q + u_{pi} D_i \\ 0 \end{bmatrix} \tag{3}$$

where σ is spatial density (mass of particles/unit volume), n is number density (mass of particles/unit volume), and u_p and e_p are the particle velocity and particle total specific energy, respectively. The particle total specific energy is related to the particle temperature T_p by

$$T_p = \frac{\left[e_p - \frac{1}{2}u_{pj}u_{pj}\right]}{c}$$

where c is the specific heat of the particles. Note for the present calculations the particles are of constant mass so that n is not critical to the calculations.

A simple two-step induction parameter method was used to model the chemical reaction of the gas.[6] The two additional equations are based on the model of Korobeinikov et al.[7] (used to approximate a diluted stoichiometric H_2/O_2 system):

$$\frac{\partial(\rho f)}{\partial t} + \frac{\partial(\rho u_j f)}{\partial x_j} = \rho\frac{\mathrm{d}f}{\mathrm{d}t} = \rho\frac{1}{\tau_{\text{ind}}} = k_1\rho^2 \exp\left(\frac{-E_1}{RT}\right) \tag{4}$$

$$\frac{\partial(\rho\omega)}{\partial t} + \frac{\partial(\rho u_j \omega)}{\partial x_j} = \rho\frac{\mathrm{d}\omega}{\mathrm{d}t} = -k_2\rho p^2 \times\left[\omega^2 \exp\left(\frac{-E_2}{RT}\right) - (1-\omega)^2 \exp\left(\frac{-(E_1+q)}{RT}\right)\right] \tag{5}$$

where f is the fraction of induction time that has passed, ω is the fraction of fuel remaining, $k_1 = 3.0 \times 10^{11}$ cm^3/(g-s), $k_2 = 1.04 \times 10^{-7}$(cm^2-s^3)/g^2, $q = 4 \times 10^{10}$ erg/g, $E_1/R = 9850$ K, $E_2/R = 2000$ K, R (the gas constant) $= 6.929 \times 10^6$ erg/(g-K), and $\gamma = 1.4$. The first step represents the induction period when radicals are being built up. An induction parameter, f, representing the fraction of induction time that has passed is convected with the fluid. Initially, f is set to 0 and ω is set to 1. As the gas heats up, such as after the passage of a shock wave, f proceeds to 1, at which time the induction period is over and the exothermic reaction [Eq. (5)] can start, with both production and consumption terms.

It is important to keep in mind that this reaction rate model does not represent the detailed reaction chemistry of actual H_2/O_2 detonations with high fidelity. The purpose of this study was to consider a simple description of a reaction system that has similarities to actual detonations. And although Matsuo and Fujiwara[8] have used this combustion model to successfully predict oscillations caused by shock-induced combustion around a blunt body, the model is certainly an approximate one because of the constant γ, c_p, and c_v employed. Therefore, the present set of reaction equations is used only as a hypothetical flowfield, which incorporates the basic features of such detonations to develop and test a numerical method for dusty detonations; its simplicity also allows a more lucent insight into the particle interaction effects.

B. Finite Element Method

The unsteady, compressible ideal reacting gas and inert particle equations can be discretized to form a conservative scheme.[9] The two-step second-order Taylor–Galerkin algorithm was used in the present study for the spatial and temporal discretization in the finite element method (FEM). In the first "predictor" step, the conserved quantities are assumed piecewise constant; for the second "corrector" step, they are assumed piecewise linear. Spatial discretization is performed via the Galerkin weighted residual method. Artificial viscosity in the form of mass diffusion is added to the second-order scheme mentioned above to obtain an inexpensive monotonic low-order scheme [note this low-order diffusion is applied with a lumped mass matrix and is different from that employed by finite-difference models of flux-corrected transport (FCT)]. From this, the low-order term contribution is combined with the high-order contribution through the FEM-FCT formulation to prevent formation of overshoots or undershoots in the conserved quantities near admissible discontinuities. To maintain strict conservation, this limiting is carried out on the element level. The limited second-order Taylor–Galerkin algorithm is employed to solve the homogeneous parts (i.e., left-hand side) of both the gas and particle equations [Eqs. (1)]. The gas/particle (interphase) coupling terms of drag and energy transfer are then calculated separately and added to the unknowns. We recently studied and validated expressions for drag and heat transfer (assuming negligible radiation) of spherical particles subjected to shock waves[1] and we have employed those expressions for the present studies (although compressibility effects are likely to be greater herein).

Grid adaptation was employed to optimize the distribution of grid points. In general, grid adaptation reduces storage and CPU requirements by 10–100 times in advection-dominated flows compared to similarly resolved fixed-grid computations.[10] Gas density (ρ) and particle spatial density (σ) were both chosen as refinement variables.[1] This is due to the high gas density gradients, which occur near shock and reaction fronts and high particle density gradients caused by variations or discontinuities in particle loading. The triangular mesh elements are refined in regions with high gradients of density to allow for a finer distribution of mesh grid points. Each local subdivision of a triangle into four triangles is referred to as a level of refinement. In regions with low gradients of density, the mesh is coarsened to efficiently use mesh grid points. In general, the method has been successfully used for computation of several nonreacting flows, including viscous flows,[10] shock diffraction flows,[11] particle-attenuated shock flows,[1,2] and shock-induced vortex dynamics.[12]

A simple two-step induction parameter method was used to model the chemical reaction of the gas.[6] Both Eqs. (4) and (5) are solved by the two-step second-order Taylor–Galerkin algorithm. The matrix inversion for Eq. (4) was the same used for Eqs. (1), which

Table 1 Detonation parameters and results for grid resolution study of single-phase conditions and two-phase simulations

Parameter[a]	S3	S3	S3	T1	T2	T3	T5
d, μm	——	——	——	80	25	25	0.1
η	——	——	——	0.75	0.75	2.70	0.75
LOR	4	5	6	5	5	5	5
$\Delta x_{\min}$	0.04	0.02	0.01	0.02	0.02	0.02	0.02
τ_U, s	——	——	——	6.8×10^{-3}	1.1×10^{-3}	1.1×10^{-3}	7.5×10^{-8}
τ_T, s	——	——	——	1.5×10^{-2}	1.4×10^{-3}	1.4×10^{-3}	2.3×10^{-8}
$\bar{C}_s$, cm/s	2.58×10^5	2.57×10^5	2.61×10^5	2.57×10^5	2.51×10^5	2.32×10^5	——
$\bar{M}_s$	4.88	4.86	4.93	4.86	4.74	4.38	——
$\bar{l}*$, cm	0.549	0.435	0.375	0.426	0.490	0.770	——
Final mode	2	2	2	2	2	1	Failure
W_L	——	——	——	1.34×10^{-6}	3.37×10^{-5}	1.21×10^{-4}	1.02×10^{-1}
Q_L	——	——	——	6.10×10^{-5}	3.65×10^{-4}	1.31×10^{-3}	4.91×10^{-2}
E_L	——	——	——	6.23×10^{-5}	3.98×10^{-4}	1.43×10^{-3}	1.51×10^{-1}
E_C	——	——	——	2.02×10^{-6}	5.05×10^{-5}	6.55×10^{-4}	1.27×10^{-1}

[a]Parameters are, respectively, particle diameter, mass loading, maximum levels of refinement, minimum element size, inertial timescale, thermal timescale, average shock velocity, average shock Mach number, average induction zone length, final mode number, work loading, heat loading, energy loading, and energy conversion.

included a three-step iterative technique based on the consistent and lumped mass matrices. However, the stiffness of the reaction rate in Eq. (5) requires that either a time-splitting or an implicit technique be used. Because of the unstructured mesh, the current study employed a point implicit scheme. For the point implicit scheme, the nonhomogeneous term in Eq. (5) is expanded in a Taylor series. The zeroth-order expansion term remains on the right-hand side; the remaining terms are moved to the left-hand side and are evaluated at the previous time step. The lumped mass matrix is used in place of the consistent mass matrix, thereby ignoring contributions from neighboring nodes and maintaining second-order accuracy.[9]

III. Discussion

A. Grid Resolution Studies

To reference the two-phase results and to examine grid resolution sensitivity, single-phase detonations in a two-dimensional tube by using the simple two-step reaction model were computed.[19] The flow was initialized with a one-dimensional Zel'dovich–von Neumann–Döring (ZND) detonation at an initial pressure of 0.1 atm and an initial temperature T_0 of 288.65 K. The flow profiles for the one-dimensional ZND were obtained by numerically integrating (with high spatial resolution) the steady-state conditions throughout the reaction zone based on a Chapman–Jouguet detonation where the Mach number M_{CJ} is given by the following equation from Ref. 6:

$$M_{CJ} = \left\{1 + \frac{(\gamma^2 - 1)q(1 - \omega_{eq})}{2\gamma RT_0}\right\}^{\frac{1}{2}} + \left\{\frac{(\gamma^2 - 1)q(1 - \omega_{eq})}{2\gamma RT_0}\right\}^{\frac{1}{2}} \tag{6}$$

where ω_{eq} is the equilibrium value of the fuel fraction, given as 0.2315. This one-dimensional steady profile (which was found to be grid independent)[9] yields an M_{CJ} of 4.8, which was used to compute the properties behind the shock wave and throughout the reaction zone.

The initial conditions for the single-phase problem are the same as those shown in Fig. 1, except there are no particles. The one-dimensional ZND wave was placed at $x = 40$ cm and allowed to travel down the tube. Perturbations in ω were placed just downstream of the detonation to allow formation of a two-dimensional detonation structure. The perturbations were introduced as two rectangular regions 0.45 cm long, which spanned the 4.5-cm width. The region in the top half of the tube was prescribed with an ω of 1.4, whereas the region in the bottom half of the tube was prescribed with an ω of 0.6.

The maximum number of levels of refinement (LOR) allowed in the computation will determine the size of the grid in regions of large gradients in ρ and σ. The more LOR allowed in the computation, the smaller the finest grid spacing ($\Delta x_{\min}$). For all cases presented in this paper, the detonation was first computed with five LOR for a distance of 15 cm (to $x = 55$ cm) from its initial one-dimensional description so that it fully traversed the above perturbation region. For both different single-phase grid resolutions (through changes in LOR) and for different particle loading test conditions, the computation

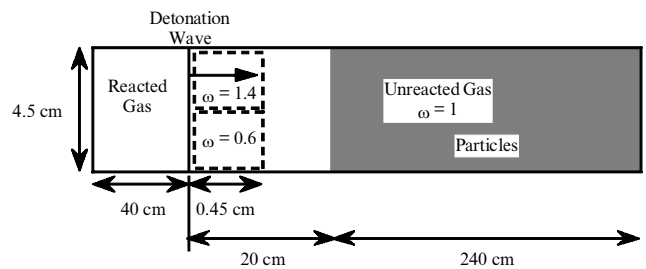

Fig. 1 Initial computational domain for dusty gas detonation simulations (not to scale).

was then allowed in proceed down the tube an additional 60 cm (to $x = 115$ cm). One reason for this two-stage temporal division was that the first 15 cm of travel was computationally intensive because of the large amount of detailed resolution required for the initial perturbation initiation. The resulting flow was deemed a *successful detonation* if it had stabilized to a specific detonation mode, with a single transverse wave termed a single-mode, two transverse waves termed a double-mode, etc. If the reaction front had separated from the shock front so that the shock speed was continually decreasing, the flow was termed a *detonation failure*.

The grid resolution study was performed with four, five, and six LOR as described in Table 1, which shows the time-averaged shock front velocities ($\bar{C}_s$), time-averaged shock front Mach number $\bar{M}_s$, time-averaged induction lengths $\bar{l}*$ (defined as the distance between the points where $f = 0.0001$ and 1.0), and the final mode; and where $\bar{C}_s$, $\bar{M}_s$, and $\bar{l}*$ data were collected along the upper and lower walls only. Note that the case prefix T is used for two-phase detonation runs and S is used for single-phase detonation runs. Additional details of the grid resolution study are given in Ref. 19.

In general, the results indicate that the macroscopic features including $\bar{C}_s$ and final mode number are grid resolved for five LOR. The induction resolution ($\Delta x_{\min}/\bar{l}*$) for five LOR was approximately $\frac{1}{20}$; this fraction is about four times smaller than that used by Taki and Fujiwara[13] (who noted a mode number dependence on grid resolution) and about the same as that used by Bourlioux and Majda.[14] The resolution of the reaction zone is similar because its size was also about 0.4 cm (this length was similar to the steady value of the one-dimensional ZND solution but rather thick compared to other two-step models). This resolution is achieved with a very modest number of grid points ($\sim$7000) as a result of the unstructured adaptive finite element technique (whole advantage becomes more profound once complex geometries are considered).[12] However, examination of $\bar{l}*$ as a function of LOR shows that this parameter (which is sensitive to the fine-scale details of the flow,[15] especially for the low-tolerance definition employed above) cannot be considered fully converged.

Grid resolution for the two-phase nonreacting case was studied in detail in Ref. 1 with fully converged results noted for shock speed.

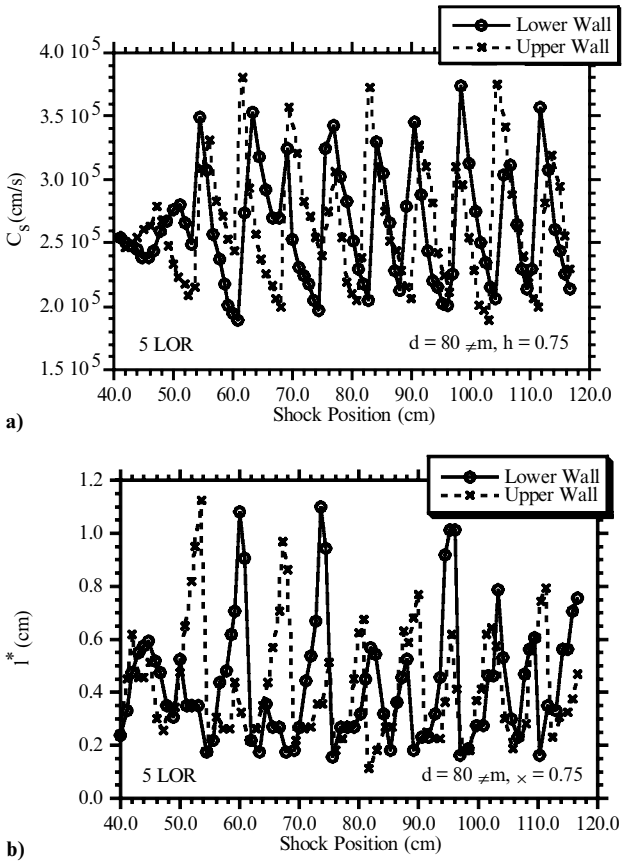

Fig. 2 History of shock velocity and induction zone length for two-phase detonation case T1.

The two-phase reacting cases (which employed five LOR) resulted in induction and reaction zones longer than that of their single-phase counterpart and thus can be considered to yield reasonably grid-independent solutions with respect to the macroscopic features. Note, even at six LOR, no numerical artifacts were noted in the solution and no changes in the basic FEM-FCT scheme were required to keep the solution stable.

B. Simulations of Particle-Laden Detonations

For the detonations with inert particles, we examined a limited number of test conditions to examine the effect such a two-phase mixture had on the detonation macroscopic features. A schematic representation of the initial conditions for the detonation problem with particles is shown in Fig. 1. The test flow used included inert glass particles with a density of 2.5 g/cm^3 and a specific heat of $7.66E+06$ erg/g-K. The particles were added in a region extending from 20 cm downstream of the initially one-dimensional detonation wave to the downstream end of the domain. This allowed the detonation to traverse 20 cm as a single-phase wave (during which time the transverse waves were able to develop based on the perturbations in ω), before reaching the uniformly distributed particle-laden region.

The particle diameter and loading were changed between cases to investigate their effect on the detonations. Table 1 presents the particle diameter, mass loading (η, the ratio of particle mass to gas mass in a given volume of the mixture), inertial time scale τ_U, and thermal time scale τ_T for all the two-phase detonations run in this study. The inertial time scale was estimated as $\rho_p d^2/(18\,\mu)$ based on Stokesian drag, which is a lower-bound approximation to the actual response time (see Ref. 9). The thermal time scale was estimated as $(C\rho_p d^2)/(3\,Nu\,k)$, where Nu is the Nusselt number and k is the thermal conductivity of the gas.[1] For the first case (T1), particles of diameter $d = 80\ \mu$m and a particle mass loading $\eta = 0.75$ were chosen. This combination was chosen as being qualitatively similar to one of the experimental conditions of Kauffman et al.[4] for which the particles had only a small effect on the detonation speed. Two additional tests (T2 and T5) investigated a reduction in the particle diameter for the same mass loading. The T5 test used particles that were so small as to make their thermal and inertial time scales much less than an interaction time between the particles and the induction zone τ_I. This interaction time scale is estimated as the $\bar{l}*/\bar{C}_s$ of the single-phase results, where the particle velocity is assumed to be a small fraction of the detonation wave speed. This yields a τ_I of 8.4×10^{-6} s, which is much smaller than the timescales of tests T1–T3, meaning that the speed and temperatures of these particles in the induction and reaction zones will be approximately equal to their preshocked conditions (zero velocity and 288.65 K). However, the particles of the T5 test will be nearly in inertial and thermal equilibrium with the surrounding gas for most of the interaction time.

For the 80-μm particles of test T1 ($\eta = 0.75$), the resulting time histories of shock velocity C_s and induction zone length $\bar{l}*$, as measured along the upper and lower walls, are shown in Figs. 2a and 2b, respectively. Oscillatory behavior is observed where sudden increases in shock velocity correspond to a collision between the transverse wave and the wall. Figure 2 indicates that the flow dynamics stabilized to a double mode (i.e., two transverse waves) with similar histories of C_s for the upper and lower walls. The same characteristics of the time histories and the double-mode propagation were found for the single-phase case (S3). Case T2, with $d = 25\ \mu$m and $\eta = 0.75$, also gave similar results of $\bar{C}_s$ and $\bar{l}*$ history.

A temporal sequence of 10 levels of density contours is shown in Figure 3 for case T2. Here we see two transverse waves just after intersecting in Fig. 3a and heading toward the lower and upper wall. As the transverse waves propagate, they locally yield in their "wake" a region of shorter induction and reaction lengths as well as a faster detonation front because of their shock strength. This is reflected in the reduced thickness of the reaction zone shown by more closely spaced density contours. The lower transverse wave has just begun to reflect off the lower wall in Fig. 3b, although not symmetrically, and both waves are moving toward the center by Fig. 3c. The cycle

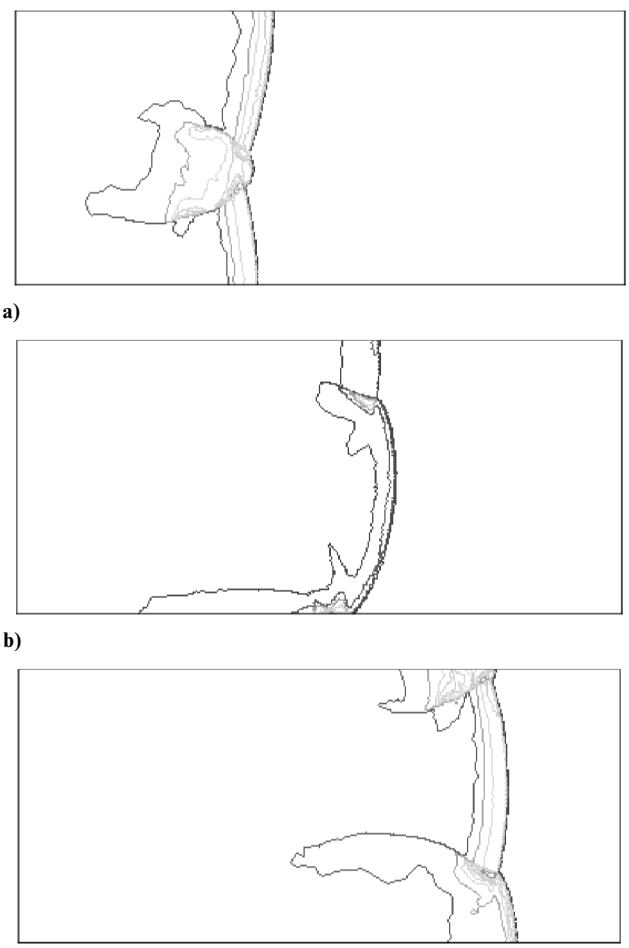

Fig. 3 Sequence of gas density contour images for case T2 (d_p = 25 μm, η = 0.75) with shock front traveling from ~87 to ~91 cm showing a double-mode detonation.

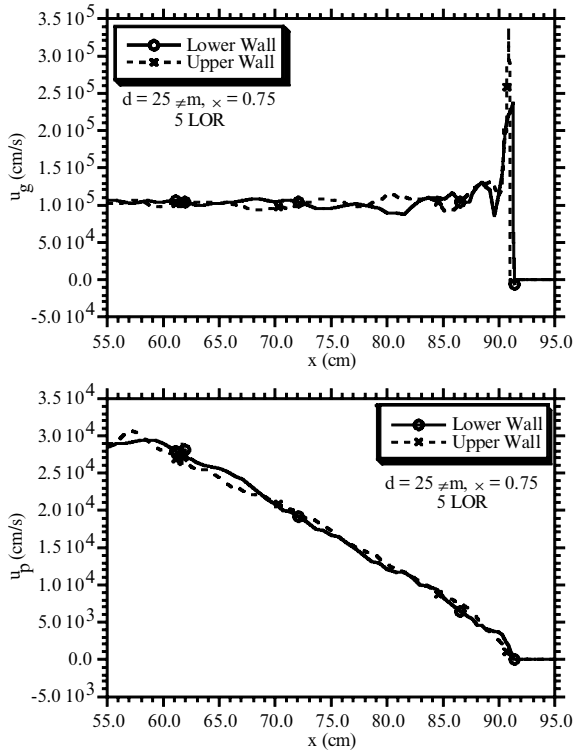

Fig. 4 Gas and particle *u* velocity along upper and lower walls for case T2 at a time step corresponding to Fig. 3c.

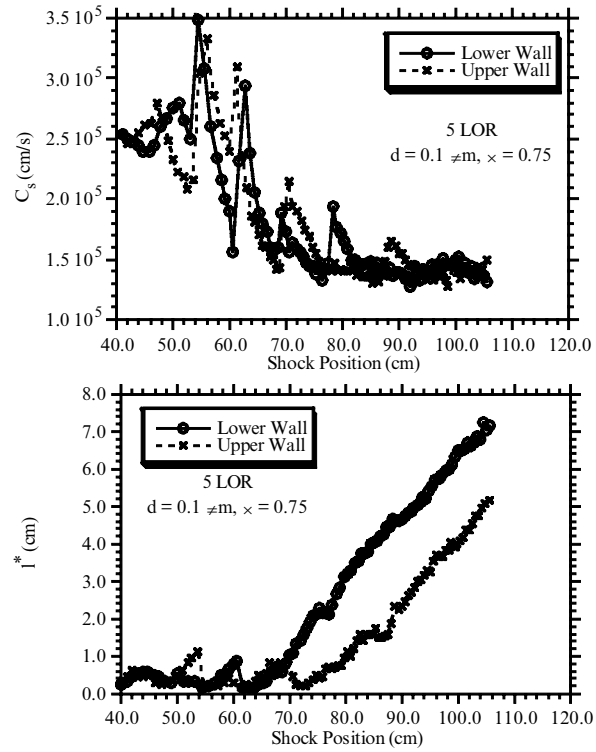

Fig. 5 History of shock velocity and induction zone length for two-phase detonation case T5.

will continue, thus yielding a successful detonation, i.e., one that continues to propagate. The same transverse wave dynamics were also noted in tests S3 and T1.

Figure 4 shows instantaneous profiles of gas and particle u velocities along the upper and lower walls corresponding to Fig. 3c of case T2. The profile of u_g looks very similar to the single-phase case (S3) at a similar time, i.e., a sharp shock discontinuity followed after a short distance by a finite reaction zone length.[9] For u_p, a lengthy relaxation zone is evident behind the detonation wave, corresponding to a similar feature in nonreacting two-phase shock flows.[1] However, the nonreacting shock case exhibited a maximum velocity difference lagging the detonation because of attenuation of the shock, whereas the present reacting case has a maximum velocity difference immediately downstream of the shock because the addition of energy into the system from the chemical reactions maintains the shock strength. In general, the T_p and T_g distributions yield profiles qualitatively similar to that for u_p and u_g.[9] Case T3, with the same particle size as T2 but greater mass loading, was found to stabilize to a single-mode detonation,[9] i.e., only one primary transverse wave within the tube at a given time. This led to a significant reduction in $\bar{C}_s$ and an increase in $\bar{l}*$; the greater times between transverse wave passage along the front also yielded increased fluctuations in both parameters.[9]

Case T5, using 0.1-μm particle diameters, exhibited detonation failure. The time histories of C_s and $l*$ are shown in Fig. 5. Both transverse waves show significant reduction in speed and frequency as they propagate. This combination is consistent with significantly reduced transverse wave strength. Beyond 80 cm, we see a rapid increase in induction length, consistent with the shock wave and reaction zone separating. For the purposes of this study, a detonation is said to fail when the reaction zone and shock wave have separated in this manner because further temporal integration should yield a deflagration wave lagging far behind an attenuating shock wave. A temporal sequence of 10 levels of density contours for detonation failure is shown in Fig. 6. At the start of the sequence, the nearly one-dimensional shock wave is seen on the right, whereas the front of the reaction zone can be seen in the lower part of the tube on the left. The remaining transverse wave is too weak to be detectable with the 10 levels of density contours. As the sequence progresses, we note that the shock wave becomes more one-dimensional (because of its reduced interaction with the reaction front) and that the reaction front movement to the right is slower than that of the shock wave.

C. Particle Influence on Shock Speed

The present numerical results for test T1 indicated nearly identical time-averaged characteristic shock speeds and very similar induction lengths compared to the single-phase case S3 (see Table 1). Comparison of the detailed wave-front propagation and time histories of the induction length and shock speeds also indicated nearly similar detonation dynamics (as described in the preceding section) with both cases yielding a mode 2 detonation. This lack of particle influence is consistent with a large particle having a relatively small particle surface area (for a fixed mass loading), where the drag and heat transfer rates are approximately proportional to particle surface area. In addition, a long particle response time indicates that the gas detonation is not significantly coupled with the particle properties.

Table 1 and Fig. 7 also show that $\bar{C}_s$ decreases slightly and $\bar{l}*$ increases slightly as particle diameter decreases (which is consistent with shorter response times) or mass loading increases (which is consistent with greater thermal and inertial capacity of the particles) and where both variations are consistent with larger surface areas. The net result is increased momentum, work, and heat transfer from the gas to the particles. For example, the addition of 80-μm particles (case T1) caused very little change in M_s. Decreasing the particle size in case T2 resulted in a drop in M_s of about 2.5%. Increasing the loading in case T3 resulted in a further drop in M_s of 7.6%. For case T5, this interaction is strong enough to lead to detonation failure. These trends are phenomenologically similar with the experimental results of Laffitte and Bouchet[3] as well as Kauffman et al.[4] Note that increasing η (test T2–T3) resulted in reduction in the detonation mode number (from two to one), but it is not definitive that a single-mode detonation is necessarily closer to failure than a double-mode detonation. Indeed, Strehlow[16] noted that similar initial conditions could lead to different mode detonations on successive tests.

Now we examine a simple equilibrium theory for the change in shock speed due to the addition of the particles. In the limit of very small particles with correspondingly very short particle inertial and thermal response times, the particles can be considered to be in equilibrium with the gas, i.e., the mixture of gas and particles can be considered as a single "mixed" fluid.[4] Thus, Eq. (6) can be used to estimate values for M_{CJ} as a function of the mass loading of the inert particles by using mixed values of γ, q, and R. For such a mixture, Rudinger[17] gives the ratio of specific heats for a mixture

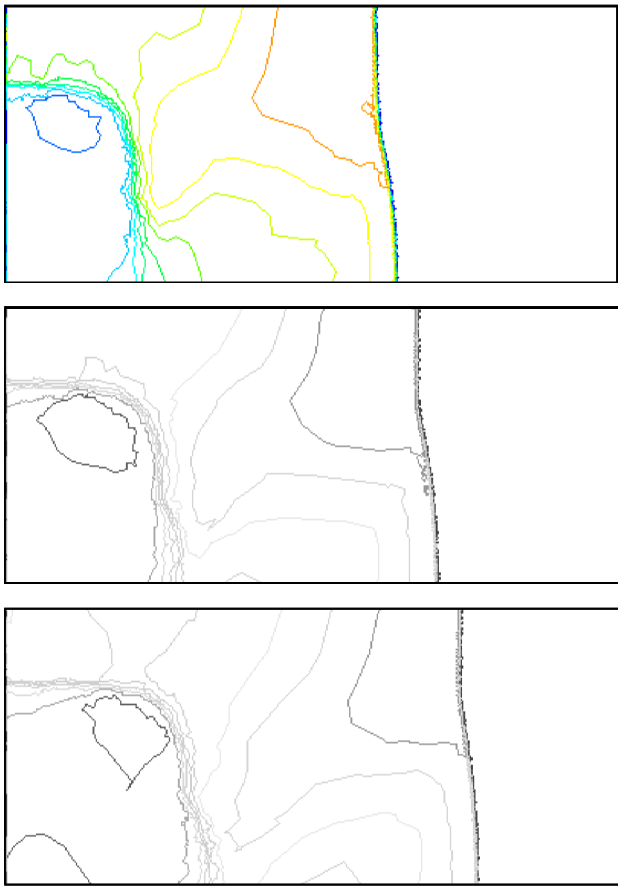

Fig. 6 Sequence of gas density contour images showing detonation failure for case T5.

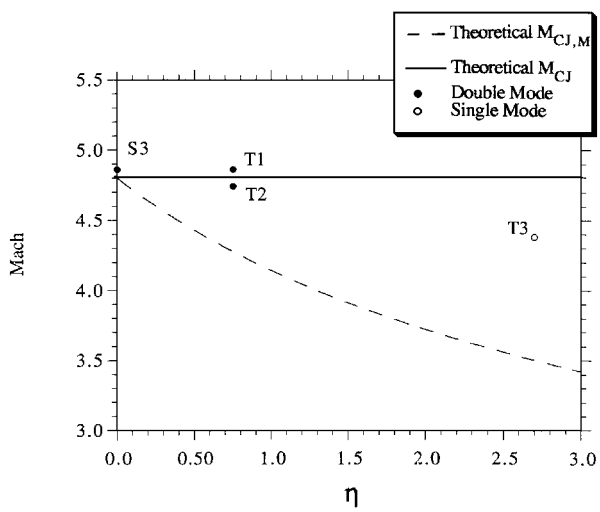

Fig. 7 Plot of theoretical $M_{CJ,M}$ (equilibrium particles) and M_{CJ} (single phase) as a function of η, along with simulation $\bar{M}_s$ for successful detonation cases.

of gas and particles γ_M, the heat of reaction per unit mass for the mixture q_M, and the gas constant R_M (see Ref. 18) as

$$\gamma_M = \gamma \frac{1+\eta\delta}{1+\gamma\eta\delta} \qquad q_M = \frac{q}{1+\eta} \qquad R_M = \frac{R}{1+\eta} \tag{7}$$

where δ is the specific heat ratio between the particles and the gas (c/c_p). Note that, because the particles are considered to be in equilibrium, the mixed value properties will be independent of particle diameter and will vary only with mass loading. Substituting Eqs. (7) into Eq. (6) gives an equation for $M_{CJ,M}$ as a function of η, which is given in Fig. 7 for the present flow conditions. Although applicable only in the limit of infinitely small particles, this theory gives an idea of the qualitative behavior one might expect in a two-phase detonation, i.e., that increasing loading will decrease the shock speed. However, this does not give information about whether the shock will be stable to such loadings or what the effects of finite inertial and thermal time scales will have on the detonation. In the limit of very large particles that do not affect flow at all, the theoretical shock Mach number would simply be equal to that of the single-phase case and this value (see Fig. 7).

The theory is compared to the results of the present simulations in Fig. 7 for the successful detonation cases. The single-phase and the mixed-flow results thus represent upper and lower bounds for the nonequilibrium simulated shock speeds. Such bounds are consistent with particles that are approximately decoupled or are approximately in equilibrium with the gas.

D. Nondimensional Particle Energy Loading

There were two expected effects of the particle's nonequilibrium behavior on the detonation physics. The first effect is due to heat conduction from the higher temperature gas to the particles and gas work done to accelerate the particles, both of which tended to decrease the temperature of the gas. The second effect is the momentum transfer due to particle drag, which attenuates nonreacting shocks as found by Sivier et al.[1] These two effects correspond to the Eq. (2) energy and momentum interphase source terms, respectively, and can be described with nondimensional parameters.

Let us first consider the energy sink terms caused by particle work and heat transfer in the induction zone, which we call energy loading (E_L). (Note that we could additionally consider the interaction in the heat release zone, but because the sizes of the two zones are about the same and because the average induction zone length and flow properties are more easily estimated, we choose to use only the induction zone.) In the induction zone, we may estimate the gas density ρ_{ind}, gas velocity u_{ind}, the drag D_{ind}, and the heat transfer Q_{ind} by assuming a normal (nonreacting) one-dimensional shock traveling at the single-phase average front speed. To nondimensionalize these sink terms in the induction zone with respect to the total amount of energy released per unit volume of unreacted gas, $\rho_{\text{ind}}(1-\omega_{\text{eq}})q$, the energy transferred per unit volume of gas per unit time in the induction zone is multiplied by the time it takes the gas to pass through the induction zone, $\tau_g = l^*/(C_s - u_{\text{ind}})$. We can thus write the energy loading as the sum of the work loading W_L and the heat loading Q_L:

$$E_L = W_L + Q_L = \frac{u_{p\text{ind}} D_{\text{ind}} \tau_g}{\rho_{\text{ind}}(1-\omega_{\text{eq}})q} + \frac{Q_{\text{ind}} \tau_g}{\rho_{\text{ind}}(1-\omega_{\text{eq}})q} \tag{8}$$

where ω_{eq} is taken as the single-phase (S3) value of 0.234. For "slow" particles (τ_U, $\tau_T \gg \tau_g$), D_{ind} and Q_{ind} can assume that the particles are at their preshocked speed (at rest) and temperature (T_0), and the gas characteristics are given by the shock-induced values when computing interphase differences for the induction zone, e.g., the relative velocity is equal to u_{ind}. The value for $u_{p\text{ind}}$ is estimated by assuming a constant acceleration in the induction zone and then taking the average value.[9] For "fast" particles (τ_U and $\tau_T \ll \tau_g$), e.g., test T5 conditions, we can assume that the particle velocity and temperature interphase differences are removed well within the induction length.[9] This yields

$$E_L \sim \frac{0.5u_{\text{ind}}^2\sigma}{\rho_{\text{ind}}(1-\omega_{\text{eq}})q} + \frac{c[T_{\text{ind}} - T_0]\sigma}{\rho_{\text{ind}}(1-\omega_{\text{eq}})q} \tag{9}$$

Figure 8 and Table 1 show the dependence of mass loading and particle diameter on energy loading for the two-phase cases. The results indicate a correlation with increasing energy loading and detonation failure; also, W_L tends to dominate E_L for large particles, whereas Q_L tends to dominate for very small particles. We hope to investigate these issues in the future by extensive parametric studies.

Similar to energy loading, the physics of drag loading can be related to a nondimensional parameter. We refer to this parameter as the energy coupling E_C, as it is intended to qualitatively represent the particle drag effect on slowing the surrounding gas under the assumption of constant total energy (the loss of energy due to the

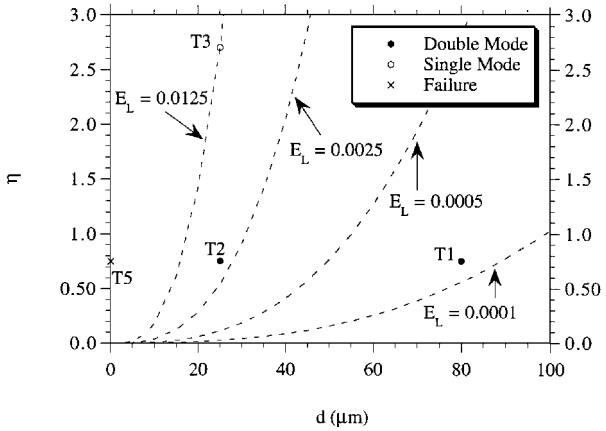

Fig. 8 Two-phase detonation cases shown as a function of d and η. Dashed lines indicate contours of constant E_L.

particles is already characterized by the energy loading). Normalizing this in a manner similar to energy loading, we have

$$E_C = \frac{D_{\text{ind}^2}\,\tau_{g^2}}{\rho_{\text{ind}^2}(1 - \omega_{\text{eq}})q} \tag{10}$$

The expression for E_C can be approximated in the same manner as E_L for slow and fast particles. For the latter, we have

$$E_C \sim \frac{u_{\text{ind}^2}\eta^2}{9(1 - \omega_{\text{eq}})q} \tag{11}$$

which gives a result independent of particle diameter [similar to Eq. (9)]. The influence of E_C on detonation success or mode number is not clear, e.g., an increase could allow higher static temperatures, which might help accelerate the detonation; however, it also could reduce the shock wave speed, which might reduce detonation strength. Future studies should obviously consider the independent variation of E_L and E_C.

IV. Conclusions

A simple two-step reacting flow model of a hypothetical stoichiometric fuel/oxygen/diluent detonation was added to an Eulerian two-phase flow solver to develop a numerical methodology for handling simulations of two-dimensional gas detonations subject to inert particles. In general, the unstructured adaptive grid methodology and point-implicit reaction treatment proved to be satisfactory at maintaining numerical stability, grid convergence of the macroscopic features, and efficient use of grid points. The resulting simulations showed that decreasing the particle diameter (while holding mass loading constant) resulted in higher drag, work, and heat loadings on the gas. When the particle diameter became very small, this trend resulted in detonation failure. Time-averaged shock speeds were found to be reduced somewhat as particle loading increased but not to the extent predicted by an equilibrium mixture between the two phases. More work is needed to understand the influences of the energy loading and energy conversion on detonation success and mode number.

Acknowledgments

This research was supported by Science Applications International Corp. (Contract 1-5-26905). Computer time was furnished by the National Center for Supercomputing Applications at the University of Illinois at Urbana–Champaign (Grant TRA950039N) and the Pittsburgh Supercomputing Center (Grant CTS960003P). The authors would like to acknowledge R. Löhner (the architect and author of FEM-FCT) for his advice as well as for the use of his code.

References

[1]Sivier, S., Loth, E., Baum, J., and Löhner, R., "Unstructured Adaptive Remeshing Finite Element Method for Dusty Shock Flows," *Shock Waves International Journal*, Vol. 4, No. 1, 1994, pp. 31–41.

[2]Sivier, S., Loth, E., and Baum, J., "Two-Phase Compressible Flow Simulations with Unstructured Adaptive Finite Elements," *AIAA Journal*, Vol. 34, No. 5, 1996, pp. 1078–1080.

[3]Laffitte, P., and Bouchet, R., "Suppression of Explosion Waves in Gaseous Mixtures by Means of Fine Powders," *Seventh Symposium (International) on Combustion* (London), Combustion Inst., Pittsburgh, PA, 1959, pp. 504–508.

[4]Kauffman, C. W., Wolanski, P., Arisoy, A., Adams, P. R., Maker, B. N., and Nicholls, J. A., "Dust, Hybrid, and Dusty Detonations," *Dynamics of Shock Waves, Explosions and Detonations*, edited by J. R. Bowen, N. Manson, A. K. Oppenheim, and R. I. Solonkhin, Vol. 94, Progress in Astronautics and Aeronautics, AIAA, New York, 1984, pp. 221–239.

[5]Kulikovskii, V. D., "Existence of Convergent Chapman–Jouguet Detonation Waves in a Dust-Laden Gas," *Combustion, Explosion and Shock Waves*, Vol. 23, No. 1, 1987, pp. 31–36.

[6]Taki, S., and Fujiwara, T., "Numerical Analysis of Two-Dimensional Non-Steady Detonations," *AIAA Journal*, Vol. 16, No. 1, 1978, pp. 73–77.

[7]Korobeinikov, V. P., Levin, V. A., Markov, V. V., and Chernyi, G. G., "Propagation of Blast Waves in a Combustible Gas," *Astronautica Acta*, Vol. 17, Nos. 4, 5, 1972, pp. 529–537.

[8]Matsuo, A., and Fujiwara, T., "Numerical Investigation of Oscillatory Instability in Shock-Induced Combustion Around a Blunt Body," *AIAA Journal*, Vol. 31, No. 10, 1993, pp. 1835–1841.

[9]Sivier, S., "Unstructured Grid Simulations of Shocks and Detonations in Two-Phase Flows," Ph.D. Thesis, Dept. of Aeronautical and Astronautical Engineering, Univ. of Illinois, Urbana, IL, May 1995.

[10]Löhner, R., Baum, J., Loth, E., and Ramamurti, R., "A Finite Element Solver for Axisymmetric Compressible Flows," AIAA Paper 89-1794, June 1989.

[11]Löhner, R., Morgan, K., Peraire, J., and Vahdati, M., "Finite Element Flux Corrected Transport (FEM-FCT) for the Euler and Navier–Stokes Equations," *International Journal for Numerical Methods in Fluids*, Vol. 7, No. 10, 1987, pp. 1093–1109.

[12]Sivier, S., Loth, E., Baum, J., and Löhner, R., "Simulations of Shock Wave Generated Vorticity," *Shock Waves International Journal*, Vol. 2, No. 1, 1992, pp. 31–41.

[13]Taki, S., and Fujiwara, T., "Numerical Simulation of Triple Shock Behavior of Gaseous Detonation," *Eighteenth Symposium (International) on Combustion* (Waterloo, ON, Canada), Combustion Inst., Pittsburgh, PA, 1981, pp. 1671–1681.

[14]Bourlioux, A., and Majda, A. J., "Theoretical and Numerical Structure for Unstable Two-Dimensional Detonations," *Combustion and Flame*, Vol. 90, Nos. 3, 4, 1992, pp. 211–229.

[15]Fickett, W., and Davis, W. C., *Detonation*, Univ. of California Press, Berkeley, CA, 1984, p. 339.

[16]Strehlow, R. A., *Combustion Fundamentals*, McGraw–Hill, New York, 1994.

[17]Rudinger, G., "Fundamentals and Applications of Gas-Particle Flow," *AGARDograph No. 222 on Flow of Solid Particles in Gases, 1996*, AGARD Fluid Dynamics Panel Meeting (Rome, Italy), AGARD, Sept. 1974, pp. 55–86.

[18]Wallis, G. B., *One-Dimensional Two-Phase Flow*, McGraw–Hill, New York, 1969.

[19]Loth, E., Sivier, S., and Baum, J., "Adaptive Unstructured Finite Element Technique for Two-Dimensional Detonation Simulations," *Shock Waves International Journal* (to be published).

K. Kailasanath
Associate Editor